# Directed Illumination of Sunlight Collimated and Observed Beneath a Lunar Lander (DISCOBaLL): Structured Illumination For a Lunar Surface Photogrammetry System

W. Callahan Eshleman*, Olivia K. Tyrrell†, Joshua M. Weisberger‡, Josiah Z. Walker§, Paul M. Danehy¶
*NASA Langley Research Center, Hampton, VA, 23681*

**A lighting system has been developed to provide structured illumination allowing photogrammetry to be performed during and after landing on extraterrestrial bodies. The system, known as Directed Illumination of Sunlight Collimated and Observed Beneath a Lunar Lander (DISCOBaLL), provides patterned lighting suitable for two- and multiple-camera photogrammetry, allowing several different measurements to be obtained including pre-landing terrain shape, visualization and localization of the ejecta sheet during landing, and post-landing terrain shape enabling quantitative measurement of plume-induced cratering. The paper explains the methodology of designing the DISCOBaLL, describes multiple prototypes, and shows the performance of these prototypes using actual solar radiation in a laboratory setting.**

## I. Introduction

Understanding the complex interactions between spacecraft rocket exhaust plumes and unimproved extraterrestrial surfaces during descent and landing is a critical issue for the future of human space exploration [1]. This so-called plume-surface interaction (PSI) involves several complex phenomena, such as particle-laden plume flow, ejecta dynamics, and erosion [2]. Potential effects of these phenomena which may induce risk include: obscuration of the landing site, damage to the vehicle, or damage to nearby assets [2]. Mitigation of these risks which will protect the spacecraft, crew, and nearby assets is paramount as spacecraft continue to increase in size and mass, with plans to return humans to the moon during the Artemis program and looking beyond to Mars. A deeper and more quantitative understanding of PSI in such landing environments will enable improvement of high-fidelity computational fluid dynamics (CFD) models [3] for predicting PSI for future landings, and mitigating the risks associated with them.

The Stereo Cameras for Lunar Plume-Surface Studies (SCALPSS) payload developed at NASA Langley Research Center is aiming to perform the first dedicated quantitative measurements of PSI-induced cratering on the lunar surface. The first payload (SCALPSS 1.0) flew on the Intuitive Machines, Inc. *NOVA-C* ("Odysseus") lander mission in February 2024, and a similar system is currently scheduled to fly on Firefly Aerospace's *Blue Ghost* lander in early 2025 (SCALPSS 1.1) [4]. The payload is designed to capture images of the erosion induced by the PSI from the lander engine(s) [4]. Using the stereo photogrammetry technique, the multiple-camera images will be used to reconstruct a 3-D depth map of the erosion profiles to better understand the extent of the plume-induced erosion. Photogrammetry is a heavily feature-dependent measurement, typically relying on high contrast of features in the images for accurate reconstruction of a 3-D shape [5]. If possible, photogrammetry is performed using coded targets or high-contrast geometric markings which are placed on or around the measurement surface to simplify image processing and obtain the lowest measurement uncertainty [6]. For lunar measurements, only natural features of the terrain will be available for detection, which may have lower image contrast due to their uniform color. The brightness and darkness of features on the lunar surface is exaggerated by the lack of an atmosphere to scatter the light. At the lunar poles, in deep natural craters, or in craters formed by the lander's plume-surface interaction during powered landing, there may be no illumination in regions where dark shadows will be cast, preventing photogrammetric measurements.

*Aerosciences Research Intern, Advanced Measurements and Data Systems Branch, Undergraduate Student, Department of Mechanical and Aerospace Engineering, North Carolina State University, Raleigh, NC, AIAA Student Member.
†Research Engineer, Advanced Measurements and Data Systems Branch, AIAA Member.
‡Research Engineer, Advanced Measurements and Data Systems Branch, AIAA Senior Member.
§Aerosciences Research Intern, Advanced Measurements and Data Systems Branch, Undergraduate Student, College of Integrated Science & Engineering, James Madison University, Harrisonburg, VA.
¶Senior Technologist, Advanced Measurements and Data Systems Branch, AIAA Associate Fellow.

A candidate solution for the issue of limited ambient lighting and image contrast on the lunar surface is to augment the SCALPSS payload with a structured illumination system. One such method currently under development for the next iteration of the SCALPSS payload (designated as SCALPSS 2.0), uses a laser projection through a diffractive optical element (DOE) to create an array of laser spots on the lunar surface which can be captured and correlated between stereo camera images. This method has been demonstrated previously by Weisberger *et al.* [7, 8]. However, designing and integrating this active illumination system, which involves class 3B/4 lasers and fragile optics, onto a lunar lander can be complicated, both mechanically and electronically. Passive illumination systems such as the one presented herein leverage the law of reflection, and the use of pinhole camera design to create a structured lighting effect comparable to that of an active illumination system for a fraction of the design time, energy, and cost.

The **D**irected **I**llumination of **S**unlight **C**ollimated and **O**bserved **B**eneath **a** **L**unar **L**ander (DISCOBaLL) technology is a passive illumination system which uses a polished paraboloidal or ellipsoidal surface discretized into rectangular facets to produce an array of light points reflected on a surface below the mounting point. When rigidly mounted on the side of a lunar lander, this variable curvature geometry allows for sunlight to be redirected to the entire area under a lunar lander as an array of points. Note that the DISCOBaLL is fixed to the lander and is not currently planned to have active articulation methods. Figure 1 shows an illustration depicting the concept of the DISCOBaLL. The sunlight reflecting off the mirrored facets illuminates the lunar surface, creating areas of high contrast over the PSI-induced crater which can be subsequently recognized by the SCALPSS photogrammetry system to enable a high-fidelity measurement.

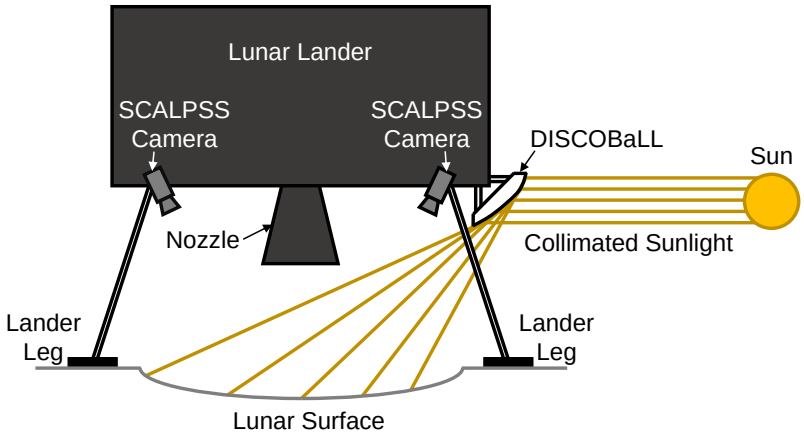


**Fig. 1 Functional diagram depicting the typical mode of operation for the DISCOBaLL concept. Collimated sunlight strikes the faceted surface and is reflected downwards below the lander to create an array of discrete reflections.**

## II. Modeling Approach

The key optical principle governing the DISCOBaLL is the pinhole camera, where an inverted image of an object is formed when light passes through a small aperture. The size of the image is dependent on the distance of the pinhole from the object and to the image plane, provided that the image plane is >100 pinhole aperture diameters from the pinhole [9]. Each of the polished facets on the DISCOBaLL acts like a pinhole camera and forms an image of the light source (in this case, the Sun) onto the reflecting surface. The image is reflected off the DISCOBaLL surface at its respective incidence angle; this angle is determined by the direction of the incoming ray of light and the normal vector of the surface of the facet. The DISCOBaLL can be thought of as one continuous variable-curvature surface such as an ellipsoid or a paraboloid which is then segmented into a specified number of facets in both the horizontal and vertical axes. The resulting surface comprises many discrete and contiguous facets, each which varies slightly in angle from neighboring facets. The variation in angle of each facet's surface normal vector occurs with respect to both the horizontal and vertical axes of the DISCOBaLL, resulting in an array of reflections on the surface below the DISCOBaLL. The brightness of each reflection is proportional to the surface area of that facet which is perpendicular to the Sun. These reflections are cast across the area under the lunar lander in a pattern determined by the shape and

curvature of the faceted DISCOBaLL, and captured within the field-of-view of the SCALPSS cameras. The bright spots of light in an otherwise dim region provide discrete, high-contrast points which can be matched between stereo images and used to accurately reconstruct the 3-D shape of the lunar surface beneath the lander. This section will provide insight into the DISCOBaLL optical surface design process conducted via a custom-built MATLAB® graphical user interface (GUI) for a flight-scale prototype.

Determining the shape of the DISCOBaLL surface is the first step of the design process. An important step when designing the surface is to consider the light striking the surface of the DISCOBaLL, and how that light needs to be directed under the lander. For each facet to transmit the same amount of optical power down onto the ground, the facets should all have an equal cross-sectional area relative to the incoming rays of light from the Sun, resulting in increasing sized facets as their angle with respect to the sun increases. To achieve the equal cross sections, a length, $l$, width, $w$, and height, $h$, of the DISCOBaLL surface must be defined. This establishes the physical size constraints for the surface of the DISCOBaLL before modifications are made to the curvature of the surface. Then, a number of facets in the horizontal direction, $N_h$, and number of facets in the vertical direction, $N_v$, must be defined. The length, width, and height are then used as bounds to create two $N_v \times N_h$ matrices, notated by $\mathbf{Y}$ and $\mathbf{Z}$. These matrices are populated with elements ranging from $-\frac{w}{2}$ to $+\frac{w}{2}$ for $\mathbf{Y}$ and 0 to $h$ for $\mathbf{Z}$. The increment in size of the elements, $\Delta_y$ and $\Delta_z$, is determined by the number of facets in each direction and the size of the surface. These $\mathbf{Y}$ and $\mathbf{Z}$ matrices are illustrated in Eqs. 1 and 2.

$$\mathbf{Y} = \begin{bmatrix} -\frac{w}{2} & \dots & y_{ij} + \Delta_y & \dots & \frac{w}{2} \\ \vdots & & \vdots & & \vdots \\ -\frac{w}{2} & \dots & y_{ij} + \Delta_y & \dots & \frac{w}{2} \end{bmatrix}, \Delta_y = \frac{w}{N_h} \tag{1}$$

$$\mathbf{Z} = \begin{bmatrix} h & \dots & h \\ \vdots & & \vdots \\ z_{ij} + \Delta_z & \dots & z_{ij} + \Delta_z \\ \vdots & & \vdots \\ 0 & \dots & 0 \end{bmatrix}, \Delta_z = \frac{h}{N_v} \tag{2}$$

A modified version of the general equation for a paraboloid or ellipsoid (denoted by the subscripts 'ell' and 'para') are represented by Eqs. 3 and 4. All of the surface modeling performed in the DISCOBaLL GUI is performed in a Cartesian coordinate system where the $+z$ axis is defined as the upwards direction, or the "height" dimension of the DISCOBaLL. The $+x$ axis is aligned with the "depth" dimension of the DISCOBaLL, and the $+y$ axis is aligned with the "width" dimension of the DISCOBaLL. These equations have been manipulated and solved for the $x$ variable of the function as the "depth" dimension of the DISCOBaLL is intended to face the sunlight. Constants for designing the curvature of the surfaces along each axis are introduced for the ellipsoid equation as $\kappa_x$, $\kappa_y$, and $\kappa_z$ and for the paraboloid equation as $a$ and $b$. Once a surface size is determined, the corresponding curvature constants are defined, and the number of facets is established, the equation is complete and ready to be evaluated. Values contained in the $\mathbf{Y}$ and $\mathbf{Z}$ matrices are made into a pair of Cartesian coordinates of the form $(y_{ij}, z_{ij})$ where $i$ represents the row and $j$ represents the column of the matrices. This is performed for the entirety of the $\mathbf{Y}$ and $\mathbf{Z}$ matrices to output a final $N_v \times N_h$ matrix, $\mathbf{X}$, shown in Eq. 5 which contains the $x$-coordinates of the surface. These equations have been manipulated such that the DISCOBaLL is established in the first and fourth standard Euclidean octants.

$$x_{ij,\text{ell}}\left(y_{ij}, z_{ij}\right) = \kappa_x \sqrt{l^2\left(1 - \frac{\left(\frac{z_{ij}}{\kappa_z} - h\right)^2}{h^2} - \frac{4y_{ij}^2}{\kappa_y^2 w^2}\right)} \tag{3}$$

$$x_{ij,\text{para}}\left(y_{ij}, z_{ij}\right) = a\sqrt{\frac{z_{ij} - \frac{4hy_{ij}^2}{w^2 b^2}}{\frac{h}{l^2}}} \tag{4}$$

$$\mathbf{X} = \begin{bmatrix} x_{11,\text{ell}\backslash\text{para}} & \dots & x_{1N_h,\text{ell}\backslash\text{para}} \\ \vdots & \ddots & \vdots \\ x_{N_v 1,\text{ell}\backslash\text{para}} & \dots & x_{N_v N_h,\text{ell}\backslash\text{para}} \end{bmatrix} \tag{5}$$

These three matrices correspond to the $x$, $y$, and $z$ coordinates of the surface's vertices. The $(x, y, z)$ coordinate pairs are then plotted in a standard Cartesian coordinate system to produce the final surface for the DISCOBaLL as seen in Fig. 2a. The plot is shown in a reference frame local to the DISCOBaLL, referred to as the "local" coordinate system. The bottom center of the surface is located on the origin of the $y$-$z$ plane at the lowest valid $x$ value on the $x$-$z$ plane of for a given set of inputs. The surface extends outwards in the positive $x$-direction. The surface is oriented such that the vectors normal to the reflective side of the surface always contain a component in the $+x$ and $-z$ direction.

The next step in the modeling process is to ray-trace the reflections from the facets. First, the DISCOBaLL's position in a global 3-D Cartesian coordinate system, referred to in this paper as the "world" reference frame, must be defined. A six-degree-of-freedom transformation can then be applied to the DISCOBaLL to manipulate the position and attitude of the surface about all three axes of the world coordinate system. From here, the coordinates of the center of each facet in the world reference frame are determined using the coordinates of the transformed surface vertices and are defined as $(x_c, y_c, z_c)$ which are the coordinates of the facet center in the world reference frame. Next, a ray of light is created to simulate collimated sunlight striking the surface of the DISCOBaLL. A vector representing the ray of light is defined which is directed from a point far off in the world coordinate system to the center of each facet. This vector is defined such that it is parallel with the local $x$-axis of the DISCOBaLL, established in a plane parallel with the world $x$-$y$ plane, and contains the same $z$-coordinate as the center of the facet off which it is reflecting. A vector like this is established for every facet on the DISCOBaLL surface. By simulating the DISCOBaLL in this way, the initial reflection pattern is representative of the Sun being located at or very near the horizon and aligned azimuthally with the DISCOBaLL. This is similar to the operating conditions expected on the lunar south pole due to the low solar elevation angles there. After the incident light vector has been established, the reflected light vector is determined using Eq. 6 where $\vec{l_{\text{ref}}}$ is the reflected light vector, $\vec{l_i}$ is the incident light vector, and $\hat{n}$ is the normal vector of the DISCOBaLL facet.

$$\vec{l_{\text{ref}}} = \vec{l_i} - 2\left(\vec{l_i} \cdot \hat{n}\right)\hat{n} \tag{6}$$

After the reflected light vector is computed, the angle between the incident and reflected ray is calculated. Should this angle be greater than or equal to 180°, there would be no physical reflection as the light ray would be parallel with the facet surface. Any vectors satisfying this condition are removed from the simulation. Once all the facet reflections have been validated, the point of intersection of the reflected light vector with the world $x$-$y$ plane is calculated using the parametric definition of a 3-D line shown by Eqs. 7-9. This calculation is performed for every facet with a valid reflection. A plot of these predicted reflections can be seen in Fig. 2b. Additionally, the DISCOBaLL and the reflection pattern are visualized together in a 3-D view of the world coordinate system in Fig. 2c to add additional visual context to the simulation. Given that the SCALPSS photogrammetry system is focusing on measuring a specific region of the lunar surface beneath a lander [4], designing the DISCOBaLL points to fall within a certain area of interest (AOI) is desirable. An AOI can be defined as a geometric region on the world $x$-$y$ plane and can be co-plotted on the predicted reflection plot as seen in Figs. 2b and 2c represented by the red circle. Note that the DISCOBaLL design present in Fig. 2 does not constitute a flight-relevant DISCOBaLL design, but a reduced version with fewer, larger facets meant to illustrate the mathematical principles at work.

$$x_{\text{ref}} = x_c + \hat{l_{\text{ref,x}}} t \tag{7}$$

$$y_{\text{ref}} = y_c + \hat{l_{\text{ref,y}}} t \tag{8}$$

$$t = -\frac{z_c}{\hat{l_{\text{ref,z}}}} \tag{9}$$

Figure 3 contains some additional enhancements which can be made to the visualization of the reflection to improve the DISCOBaLL iterative design process. The design shown in Fig. 3 is more flight-relevant than the basic design shown in Fig. 2; it features a larger quantity of facets in order to create a denser pattern of reflections on the $x$-$y$ plane, smaller facet sizes, and a smaller overall DISCOBaLL form factor. In the Fig. 3, the DISCOBaLL has been translated in the world reference frame upwards by ~1 m, moved into the third quadrant of the $x$-$y$ plane, and rotated to mimic being mounted off the side of a lunar lander. Its position in the world $x$-$y$ plane is denoted by the blue + symbol plotted on Figs. 3c and 3b. A setting can be turned on which will determine if a reflection is inside or outside of the AOI and remove the reflection from the plot if the reflection falls outside of the target region. This can be seen in Fig. 3c as the number of reflected points does not match the number of facets on the DISCOBaLL surface and reflected points on the

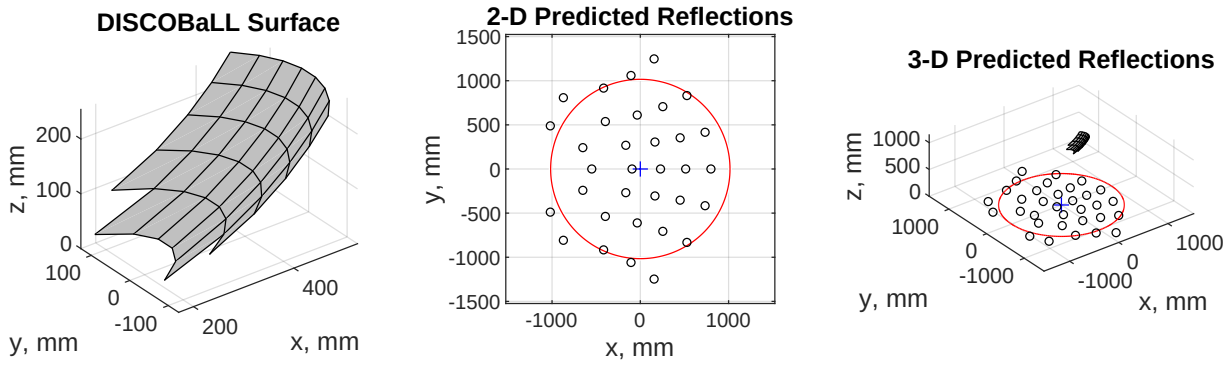


(a) (b) (c)

**Fig. 2 Plot of the DISCOBaLL surface in the "local" coordinate frame, (a). The reflective surface is pointed away from the reader in this view. Plot showing the reflection pattern from the DISCOBaLL onto a flat plane, (b). The red circle is a defined "area of interest" which represents a to-scale physical space on the world $x$-$y$ plane. A combined 3-D plot showing the DISCOBaLL surface and the reflected points, (c).**

outside of the AOI (denoted by the red circle) are not shown. The facets which correspond to the reflections that miss the AOI will be highlighted in red, shown in Fig. 3a. These unnecessary facets can be excluded from the design in CAD software after the DISCOBaLL has been exported from the developer GUI, or the equation defining the surface of the DISCOBaLL can be further manipulated to optimize the design and realize mass/volume savings.

Another feature of the developer GUI is plotting the predicted size of the reflected image of the Sun on the world $x$-$y$ plane. The size of the image of the Sun can be quickly estimated through the formula in Eq. 10 where $D_{\text{ref}}$ is the diameter of the reflected image of the Sun, $D_{\text{Sun}}$ is the equatorial diameter of the Sun, $d_c$ is the distance from the facet center to the reflection, and $d_{\text{s}\rightarrow\text{e}}$ is the distance from the Sun to the Earth. Once this has been calculated, a circle is plotted centered on the reflection coordinate with the calculated diameter for that given reflection. Figures 3b and 3c showcase the plotting of the predicted reflection size. A more robust model which would take into account the position of the astral body the DISCOBaLL will reside on relative to the Sun, the elliptical shape of the reflection on the ground, and the ability to project the reflected points onto a non-flat surface would improve the fidelity of these simulations.

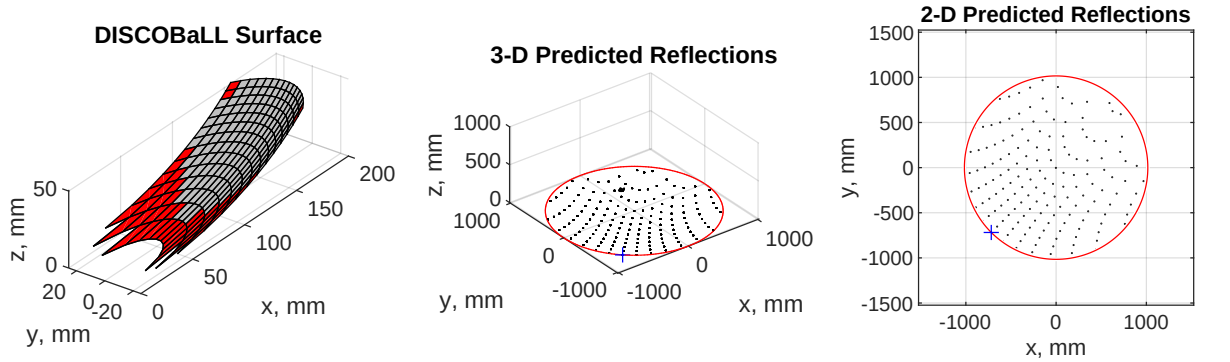


(a) (b) (c)

**Fig. 3 Predicted performance of a practical DISCOBaLL design: (a) The surface of the DISCOBaLL in the local coordinate system with the facets whose reflections miss the AOI highlighted in red. The reflective surface is pointed away from the reader in this view. (b) Plot showing the predicted reflections of the DISCOBaLL with the AOI limiter and real reflection size prediction enabled. (c) Plot showing the 2-D representation of the world coordinate system containing the DISCOBaLL and the reflected points.**

$$D_{\text{ref}} = D_{\text{sun}} \frac{d_c}{d_{\text{s}\rightarrow \text{e}}} \tag{10}$$

As discussed earlier, the angle of a reflected ray of light is dependent upon the angle between the incident light ray and the normal vector of the reflective surface. As the incident ray changes, so does the reflected ray and therefore the position reflection on the ground. Nominal operations for the SCALPSS flight payloads are set to occur over a range of a few Earth days [4]. As the Sun traverses along the horizon of the lunar south pole, the reflected points of light from the DISCOBaLL will traverse over the ground. In turn, this will enable the photogrammetry system to effectively collect a new set of measurement points every time the Sun's position changes relative to the DISCOBaLL, provided that the points do not eventually overlap with previous point locations. The designer GUI ephemeris code is able to simulate changes of the position of the Sun in the sky. An azimuth and elevation angle can be applied to the sunlight vector and the reflection pattern on the ground responds accordingly. The code can also predict the cumulative traversal path of the reflections as the Sun traverses across the lunar sky for any period of time. Figure 4 contains the same flight-relevant DISCOBaLL design from Fig. 3 with a solar ephemeris applied. The ephemeris file was created using the NASA Jet Propulsion Laboratory Horizons program based on a defined observer location of the lunar south pole and astral body of the Sun. The ephemeris contained the azimuth and elevation angles of the Sun relative to the observer location at midnight UTC for one calendar week. The reflections can be seen concentrating over the left side of the AOI on the first day, distributing more evenly over the entire AOI three days later, and concentrating again on the right side of the AOI on the last day. The movement of the reflections across the surface and subsequent image captures at the additional points in time over the three different days effectively triples the number of measurement points obtained with no additional mechanisms necessary. A more optimized design might illuminate a new location on the ground several times a day for a week, dramatically increasing the number of measurement points collected for the photogrammetric surface reconstruction and improving the resolution of the measurement.

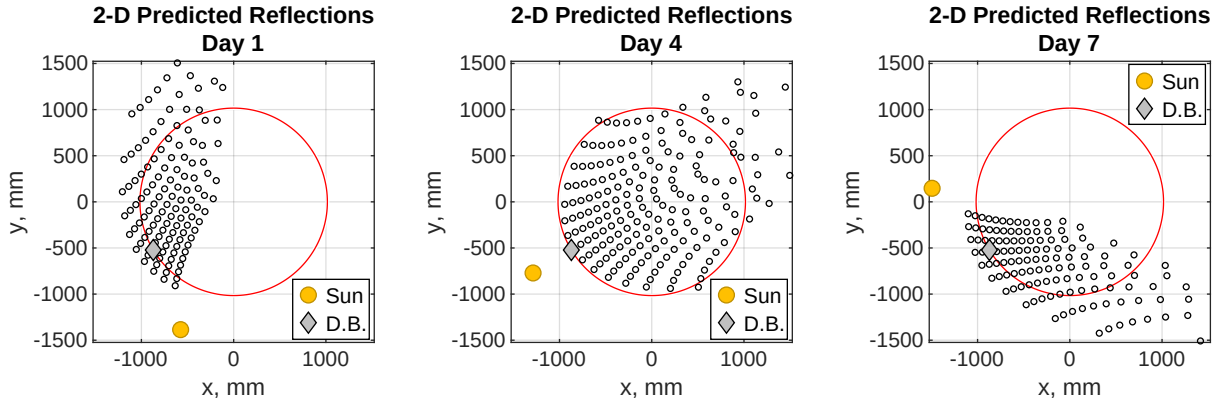


**(a)** **(b)** **(c)**

**Fig. 4 Predicted reflection pattern of the DISCOBaLL using solar ephemeris data for a lunar south pole landing site over a week: (a) Day 1, (b) Day 4, and (c) Day 7.**

## III. Prototyping

Developing a DISCOBaLL design for a lunar flight opportunity requires consideration of several factors, including: the geometry of the lunar lander, the landing site, landing date/time, and the measurement area of interest on the lunar surface. The DISCOBaLL designer GUI detailed in the previous section can be used to determine a mirror surface geometry which produces the desired reflection pattern for this combination of factors. The MATLAB®-generated surface plot of the faceted mirror geometry can be exported from the designer GUI as a stereolithography (STL) file and imported into a standard CAD software, where it can be converted to a 3-D solid model of the DISCOBaLL. From

there the model can be 3-D printed or machined and evaluated iteratively to optimize quality and performance as a passive light source reflector. Modifications for mechanical integration onto a flight vehicle, such as mounting hardware and structural features to withstand launch and landing loads, can also be incorporated to mature the design towards flight-readiness.

In the current work, various low-cost plastic 3-D printing methods were used to create initial prototypes of the DISCOBaLL. The faceted surfaces were wrapped in a reflective tape to emulate the reflectivity of a polished piece of metal. While these initial prototypes proved useful in qualitative validation of the predicted reflected dot patterns for a given design, they unevenly scattered light due to striations in the surface finish of the 3-D printed material. As a result, it was difficult to extract quantitative information such as reflected spot size and intensity from these prototypes.

To assess manufacturability and ultimately progress the design towards flight-readiness, a portion of a DISCOBaLL was milled on a 5-axis Computerized Numerical Control (CNC) machine. The portion was milled first out of aluminum and then stainless steel. In an effort to achieve the most mirror-like surface finish, the prototypes were subject to various cutting tools, milling patterns, and polishing methods. Machining and material factors which contribute to the performance of a DISCOBaLL element include: surface roughness, surface finish, angle and size of edges between adjacent facets, and the overall size of the facets. The need to carefully control each of these parameters during the manufacturing phase proved challenging; a select few of these parameters were tested in initial prototyping, and photographs of the resulting DISCOBaLL portions are shown in Fig. 5. A single, relatively simple DISCOBaLL design was used for all three prototypes shown, consisting of a sub-section of a larger design generated in the MATLAB® designer GUI. The selected design featured an ellipsoidal geometry with curvature constants $\kappa_x$, $\kappa_y$, and $\kappa_z$ of 355.6 mm (14”), 152.4 mm (6”), and 203.2 mm (8”), respectively, and was at full-scale approximately 203.2 mm (8”) long and 101.6 mm (4”) wide. Each facet was approximately $6.35\left(\frac{1}{4}\text{”}\right) \times 6.35\left(\frac{1}{4}\text{”}\right)$ square. From this design, a $\sim 2\text{”} \times 3\text{”}$ piece was “sliced” out of the model and converted into a 3-D solid CAD file using the process described earlier in this section. That file was then uploaded into the CNC mill software and the part was cut from stock material. The so-called Version 1.0a in Fig. 5 was initially created using aluminum stock as a way to test out the mill program. It was cut using a single-pass pattern and was unpolished. The surface finish and reflectivity of Version 1.0a was poor; furthermore, aluminum was rejected as a potential flight material owing to its susceptibility to corrosion, scratching and oxidation. Stainless steel (316L) was ultimately selected as a more flight-capable material that was relatively easy to manufacture, polish, and resist corrosion or damage. Version 1.0b was produced using 316L stainless steel and a circular brush-cut pattern for the milling process. It was polished by hand with jeweler’s rouge after the milling process was completed. Despite achieving a relatively smooth surface finish, the cutting pattern removed material and produced a circular pattern over the facets, such that the individual square facets would not reflect images of the light source as intended. Version 1.0c was produced using the same 316L stainless steel but was milled with a single-pass cut tooling pattern, and polished using the same method as Version 1.0b. This resulted in a much more precise surface finish and high reflectivity, demonstrated by the reflection of the phone camera which is clearly seen in the rightmost image of Fig. 5.

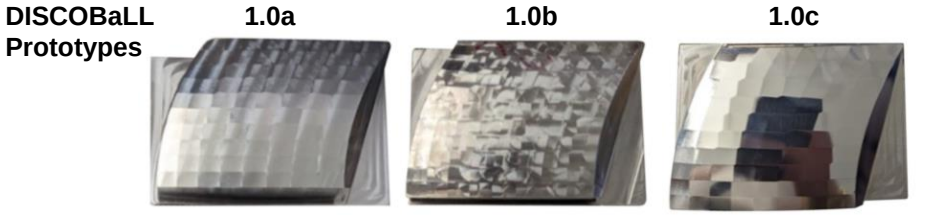


| | | | |
|---|---|---|---|
| Material: | Aluminum | Stainless Steel | Stainless Steel |
| Cutting Pattern: | Single-Pass Cut | Circular-Brush Cut | Single-Pass Cut |
| Polish: | Not Polished | Polished | Polished |

**Fig. 5 Three different DISCOBaLL prototypes manufactured on a 5-axis CNC mill. All three prototypes possess the same DISCOBaLL surface design, but are made from different materials or were milled by different tools.**

After establishing a manufacturing process which could achieve highly reflective and distinct facets, a secondary DISCOBaLL prototype design was created which would allow for the evaluation of facet size. When developing flight

hardware and instrumentation, the conservation of size, weight, and power (often referred to collectively as SWaP) is critical for cost and propellant savings; therefore, smaller facet sizes will enable a smaller form factor in the design to realize payload mass savings. Another benefit of having smaller facet sizes is that a larger number of facets can be fit into a given volume resulting in more dots of light being reflected onto the lunar surface and providing a significant enhancement in the spatial resolution and/or total coverage area of the measured terrain. In practicality, both of these features can be traded to optimize for a sufficiently robust measurement that still keeps the payload SWaP within an allocated budget. As explained in the previous section, according to the pinhole camera concept, the reflected spot size depends only on the relative distance from the object (the Sun) and the image plane (the lunar surface) to the pinhole (the DISCOBaLL), therefore, facet size should not have an effect on reflected spot size. Instead, the brightness of the reflected spots will be highly dependent on the facet surface area. Since the detection of the reflected spots in the SCALPSS payload camera images is paramount to using them in feature correlation and eventual reconstruction of the plume-induced erosion, the reflected spots should be sufficiently bright to have contrast against a potentially partially-illuminated terrain (by scattered or ambient sunlight). Furthermore, the manufacturability of repeated adjacent facets limits the minimum achievable size. Consequently, a trade study of facet size vs. manufacturability and reflected spot intensity was performed using a Version 2.0 DISCOBaLL prototype, shown in Fig. 6. This 2.0 prototype design was $\sim$ 50 mm $\times$ 50 mm (2" $\times$ 2") square and featured four distinct quadrants each having a different square facet size (2 mm, 3 mm, 4 mm, and 5 mm). A high-quality surface finish was achieved on all four facet size quadrants of the prototype, and clear visual delineation between adjacent facets can be observed in Fig. 6. Evaluation of these prototypes as passive sunlight reflectors is discussed in the next section.

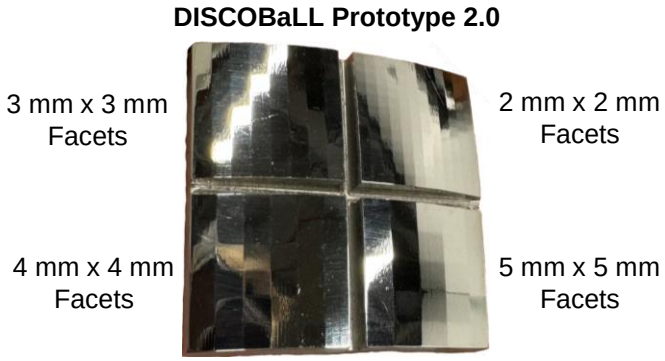


**Fig. 6 Image of the DISCOBaLL prototype 2.0. The $\sim$ 50 mm $\times$ 50 mm 316 stainless steel surface was divided into four quadrants. Facet sizes manufactured were 2 mm, 3 mm, 4 mm, and 5 mm. The highest resolution can be seen in the top right corner where each facet is 2 mm x 2 mm.**

## IV. Laboratory Testing

The 316 stainless-steel single-pass cut, polished prototype (Version 1.0c) was tested in a laboratory setting to evaluate the projected dot pattern, the dot brightness as perceived by the camera, and the ability for the DISCOBaLL to facilitate a useful photogrammetry measurement, as well as the implications of the manufacturing and polishing process on each of these criteria.

The Version 1.0c prototype was set up to project light onto the surface of a large papier-mâché lunar crater model previously used by Tyrrell *et al.* for measurement accuracy validation for the SCALPSS 1.1 flight configuration [10]; therefore, the shape of the crater was precisely known. A white light source was placed several meters away and used in combination with a Fresnel lens to simulate the collimated light of the Sun striking the surface of the DISCOBaLL. Two small circular mirrors were also mounted near the DISCOBaLL and used as an ideal reflectance comparison for the perceived brightness measurement. A two-camera photogrammetry system using the same cameras as SCALPSS 1.0/1.1 systems was then set up and used to image the crater from a $\sim$1.5 m distance, chosen to replicate a flight-relevant scale.

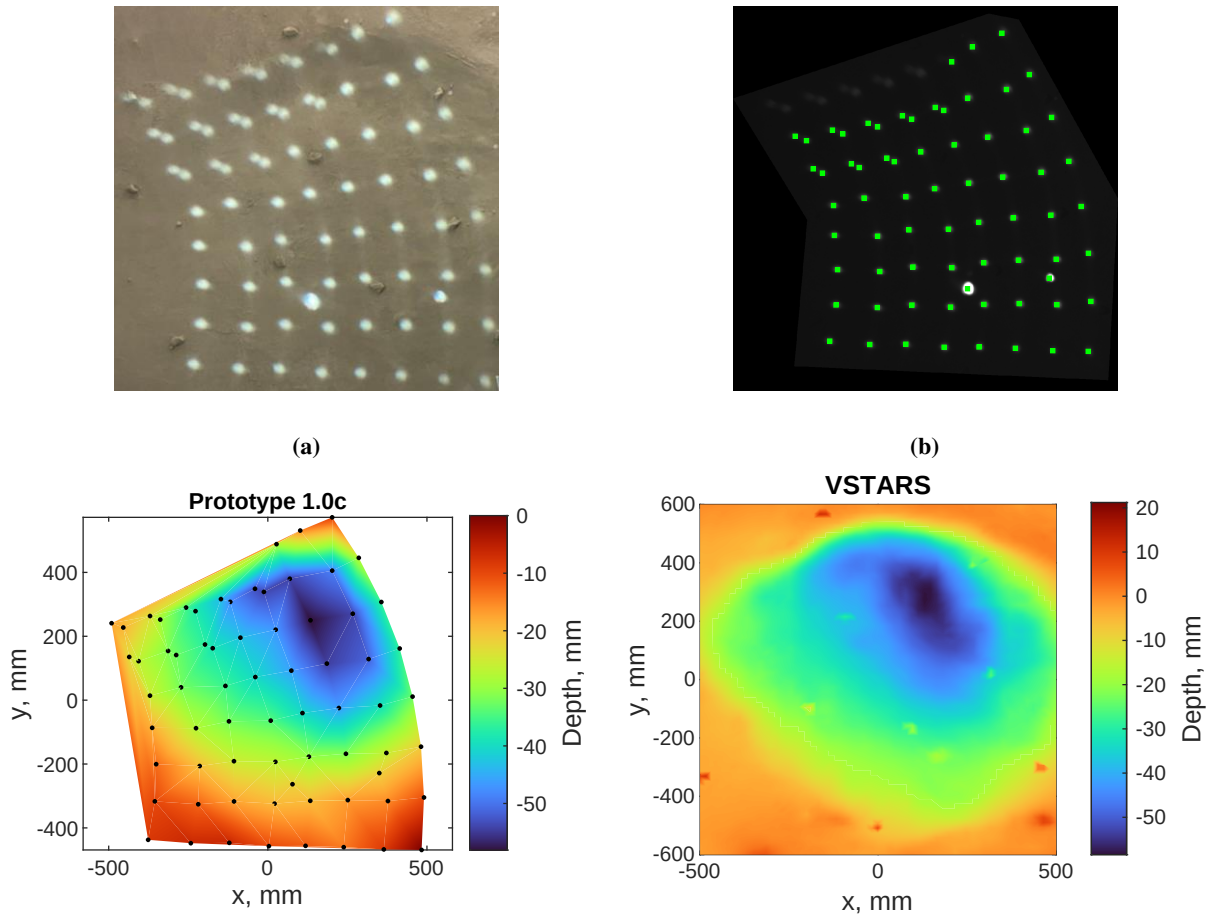


**Fig. 7 Results of laboratory testing of DISCOBaLL prototype Version 1.0c. (a) Image of the reflections on the lunar crater model acquired with a cellphone camera. (b) Detected centroids for the reflected points captured using SCALPSS stereo cameras. (c) Plot showing the measured shape of the crater model using only the DISCOBaLL 1.0c reflected points. (d) Plot showing a high-fidelity photogrammetric measurement of the crater model for comparison to (c).**

At the beginning of the experiment, a set of images containing a calibrated checkerboard target was taken on the two cameras to derive the exterior orientation of the camera pair using the MATLAB® Stereo Camera Calibrator from the Computer Vision Toolbox. Another image set was taken at various exposures for each camera with the lens cap on to capture the dark noise from the camera sensors (to be later subtracted from the signal images). At this point data acquisition could begin. For every data set, a set of signal images and background images were taken. Signal images indicate an image with the DISCOBaLL and mirror reflections on the crater model. A background image is an image of the crater model with the reflections from the DISCOBaLL and mirrors blocked. The crater was moved back and forth to a variety of positions and images were acquired at every position.

To process the measurement of the crater at a given distance from the DISCOBaLL, the signal images, background images, and dark noise image sets were individually averaged together and then the dark noise and background were subtracted from the signal image. Figure 7a shows an image taken on a cellphone camera of the DISCOBaLL and mirrors reflecting on the lunar crater model. Figure 7b shows an image taken using a SCALPSS camera of the reflected spots on the crater model. The green squares seen on the image indicate the centroids of the reflected light spots, identified using image thresholding and centroid finding algorithms in MATLAB®. Matching centroids detected in each single image for the stereo pair were then used to calculate a disparity in the rectified plane containing both images. The disparity is the number of pixels between each matching pair of points in the rectified image, which can be mapped to

a depth value using the stereo calibration parameters for the camera system. For more information about the image processing methods used to generate the depth and shape measurements, see Ref. [7]. The resulting shape measurement of the crater model using only the detected points from the DISCOBaLL reflection is plotted in Fig. 7c. A higher-fidelity measurement of the crater obtained using a commercial photogrammetry system detailed in Ref. [10] is shown in Fig. 7d for comparison. The computed depth values in the region of the crater model measured using the stereo image data of the DISCOBaLL reflected points demonstrates agreement with the high-fidelity measurement. This shows that the DISCOBaLL can be used with the SCALPSS system to make an acceptably accurate crater depth measurement in low- to no-ambient illumination conditions, despite having a coarser resolution than would be expected from a uniformly illuminated, feature-rich set of images. Further conclusions and lessons learned from the DISCOBaLL Version 1.0c prototype testing will be discussed in Section V.

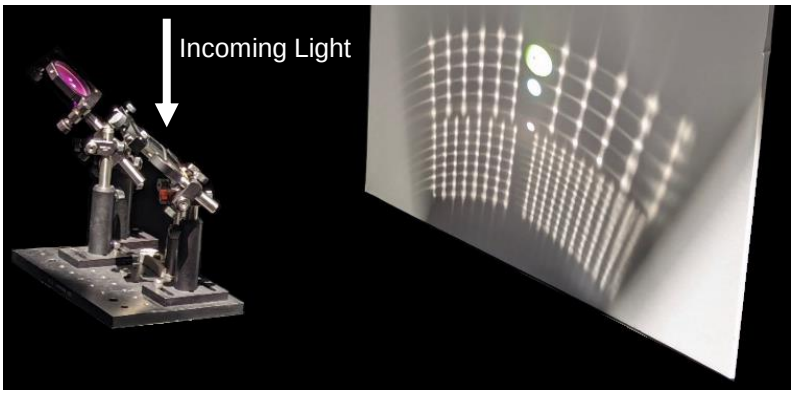


**Fig. 8 The DISCOBaLL prototype Version 2.0 testing apparatus can be seen on the left side of the image. It contains four optical mounts holding the prototype 2.0 and three circular mirrors of varying diameter. The white board where the reflections were projected can be seen on the right side of the image, illuminated by the reflections from the DISCOBaLL prototype and the mirrors. Sunlight enters from the skylight above.**

During the tests and data analysis for the DISCOBaLL prototype Version 1.0c, it was determined that the white lamp and Fresnel lens combination was not sufficient for simulating the pinhole camera effect described previously; the Fresnel lens was not perfectly collimating the light from the lamp. Therefore, the Sun was used as the next light source for the prototype Version 2.0 testing. The goal of the prototype Version 2.0 testing was to determine the effect of facet area on perceived intensity and reflection size. A "penthouse" laboratory at NASA Langley Research Center's Measurement Sciences Laboratory (MSL) contains windowless skylights ports that can be opened allowing sunlight to directly illuminate the DISCOBaLL. This capability was used for all subsequent testing described in this paper. Figure 8 shows the experimental set up of the DISCOBaLL prototype Version 2.0 testing. For this experiment, the same camera calibration and image acquisition process was followed as prototype Version 1.0c testing. However, the crater model was not initially used as the test surface; instead, a flat white poster board was used to limit the amount of distortion each reflection encountered. The DISCOBaLL was held in an optical mount secured to an optical breadboard with three other mirrors with diameters of 0.5", 1", and 2". These mirrors were included in the experiment to validate the reflection size measurement and ensure that the DISCOBaLL reflection was working in the aperture/pinhole regime imaging the Sun and not as a square reflection of the faceted surface. The skylight in the laboratory was opened for testing on a sunny, clear day where the sun was directly over the MSL. This allowed the sunlight to enter the room from above and reflect off the DISCOBaLL and mirrors onto the white board material. The experiment was conducted with the flat board located at a distance of ~0.61 m (~24") and ~1.83 m (~72") from the testing apparatus. Multiple data sets were taken at a variety of exposures to ensure sufficient signal of the DISCOBaLL spots and the mirrors. For the DISCOBaLL spots, the exposure time used was 205.04 $\mu$s at a distance of 0.61 m and 1253.25 $\mu$s at a distance of 1.83 m. This exposure had to be changed due to the coating on the surface of the flat board which was more or less reflective depending on the observer's angle relative to the board. The data sets for the mirror spots were acquired at an exposure of 45.54 $\mu$s. The post-processing of the data from these experiments followed the same process as the prototype Version 1.0c data.

Additionally, an experiment was performed to examine the Sun traversal feature of the DISCOBaLL. The photogrammetry system was set up and calibrated exactly as described in the previous experiments with the various

prototypes. Background images and dark noise images were taken at the beginning of testing. The penthouse skylight lab at NASA Langley's MSL was again used to conduct this experiment. The DISCOBaLL apparatus was set up the same as shown in Fig. 8 but without the circular mirrors. Next, the lunar crater model used in the prototype Version 1.0c testing was positioned roughly one meter in front of the DISCOBaLL (similar to the expected scale for a flight configuration). As the Sun moved across the sky all of the DISCOBaLL reflections moved on to the crater. The photogrammetry system was set to acquire data at 1 Hz and was left to image the DISCOBaLL until the sunlight had completely moved off of the DISCOBaLL (approximately 23 minutes). The images were processed in the same way as previously described to extract depth data, and the photogrammetry measurements from the different positions of the reflections were concatenated to obtain a higher-fidelity measurement of the crater model than one static image set would have produced. Detailed analysis and presentation of the results from DISCOBaLL prototype 1.0c and 2.0 testing are presented in the next section.

## V. Results

Testing from the DISCOBaLL prototype Version 1.0c proved the ability of the DISCOBaLL to create high contrast discrete reflections and that a simple DISCOBaLL reflection pattern could be used to create a coarse but accurate surface reconstruction measurement, shown in Fig. 7c. Due to the low density of reflections produced by the DISCOBaLL, some detailed features of the surface acquired in prior measurements were not captured. This observation can be seen in the disparity of the limits of the "Depth" color bar axis between Fig. 7c and Fig. 7d. For example, small rocks placed over the surface of the crater model were not captured by the low-resolution DISCOBaLL measurement. A larger quantity of facets is desirable, resulting in a denser arrangement of reflected dots and an ultimately higher-resolution measurement. This observation led to the development of the prototype Version 2.0 which will be discussed later in this section.

More observations were made during testing about effects of the modeling, design, and manufacturing process on the performance of the prototype Version 1.0c. When the DISCOBaLL surface is exported from MATLAB® the software meshes all of the polygons as an amalgamation of smaller triangles. Due to the large size of the facets on the DISCOBaLL prototype Version 1.0c and the curvature of the outer edges of the surface, some of the meshed triangles composing the facets were exported with a slight angular offset. This angle was significant enough to be recognized by the machining programming software and some of the facets were split into two surfaces at a slight angle relative to one another. These split surfaces produced two reflections which can be seen in the top left corner of Fig. 7a. While some of the spots could still be recognized, the splitting of the surfaces reduced the intensity of the reflections making detection of the points and depth data reconstruction more challenging at those regions. This meshing issue was eliminated in future designs of the GUI.

Another side effect of the manufacturing process which was observed in the prototype Version 1.0c testing is the small lines of light which run between the reflections. Due to the finite size of the edges between the facets, light is scattered off the edges which produces "bridges" running between the reflected spots. While these did not significantly impact the results of the prototype Version 1.0c testing, they did highlight the importance of controlling the tolerance of the machining and polishing. As those facet edges become larger or more rounded, more light is scattered over the surface. This may lower the contrast of the reflections against the target surface, or prevent single points from being identified, adversely affecting the measurement.

Testing of the DISCOBaLL prototype Version 2.0 was more informative with regard to the underlying physics employed by the DISCOBaLL. As described in Section IV, images were acquired of the DISCOBaLL reflections on a flat plane located at distances of 0.61 m and 1.83 m. Adverse lighting effects from the surface coating of the flat panel required the exposure of the cameras to be changed between the two distance to prevent saturation of the reflected points in the images. For this reason only the 1.83 m distance dataset was analyzed for the intensity versus reflective surface area investigation, while both data sets were used to evaluate the reflection size versus the reflective surface area. As mentioned in Section IV, the data was acquired by individually averaging 100 signal, background, and dark noise images taken at the exposure of the signal and background images. The dark noise and background were subtracted from the signal image.

To begin the intensity and spot size analysis, an image thresholding algorithm was employed to filter out any additional noise and detect the locations of the DISCOBaLL reflections in the image. Once thresholded, the image was binarized and the centroid of the DISCOBaLL reflections in the image plane were found. This process was repeated for each facet size. However, due to the light "bridging" effect between the reflections and the difference in the reflection

intensities across the facet sizes, one single thresholding value could not be used to reliably find the centroid of every reflection. For this reason, the image thresholding was only used to find the centroid of the reflected regions and was not used to examine the reflection sizes. Errors in the machining process produced a very rough surface along the edges of the prototype. This caused some of the reflections at the edges of the reflection pattern to be very diffuse and appear differently from the rest of the reflections. The diffuse reflections from both the "bridging" effect and the edge region surface finish effect can be observed in Fig. 8, especially in the 2 mm x 2 mm facet size points. Forty-eight 2 mm x 2 mm facet points were removed and five 5 mm x 5 mm facet points were removed. These points were manually removed from the data set to prevent skewing of the reflected size results.

After finding the centroids, a horizontal line of pixels was sampled across every reflection to find the reflection profile. A horizontal line of pixels was chosen instead of other profile-scanning methods because the light bridging between the facets was most noticeable in the vertical direction. For the 2 mm facet size, 10 pixels on either side of the centroid were sampled. For the 3 mm, 4 mm, and 5 mm reflections 15 pixels on either side of the centroid were sampled. The discrepancy in the number of pixels sampled is due to the density of the reflections. The 2 mm reflections were spaced so closely together on the board that sampling with 15 pixels on either side of the centroid sampled multiple reflections. Once every valid facet reflection was sampled, the reflection profiles were aligned by their peak intensities and the profiles were averaged together. The mean and standard deviation of the profile was calculated for each facet size and is plotted versus the facet area in Fig. 9. The Fig. 9 subplot insets correspond to the average intensity profile of the respective facet sizes.

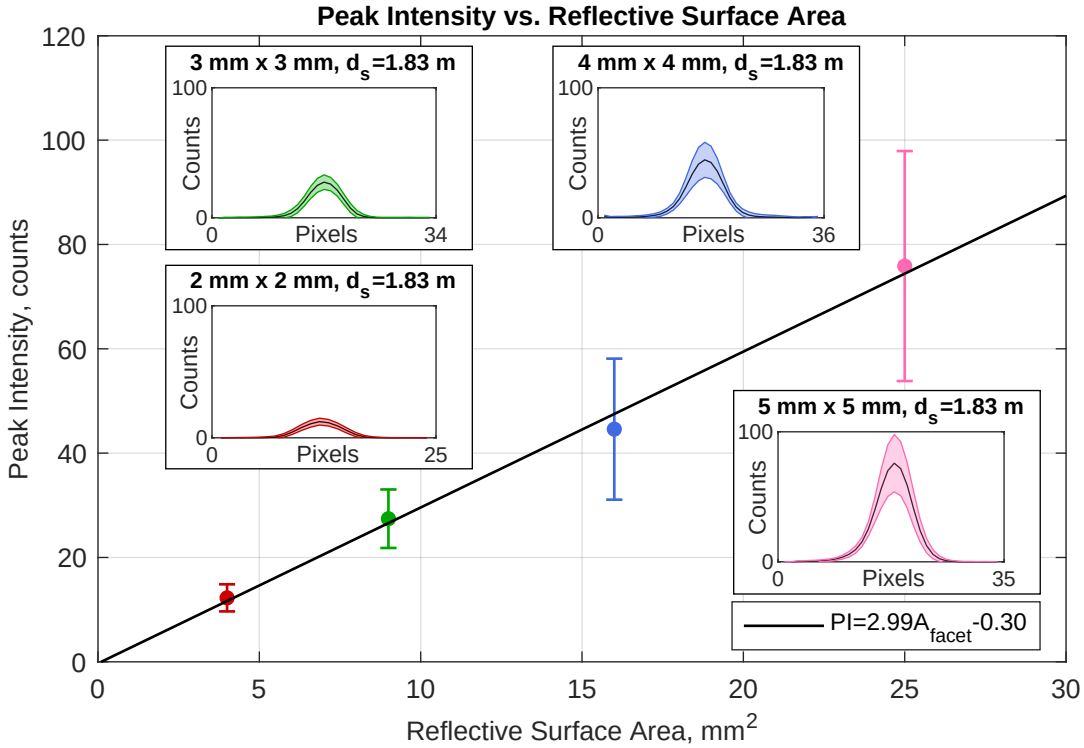


**Fig. 9 Plot of the average peak intensity for each DISCOBaLL prototype Version 2.0 facet size's reflection versus the area of the facet. Each point corresponds to the average maximum intensity value of the respective facet size. The subplots represent the mean intensity profile of each reflected facet size and are color coordinated with the points on the main axis.**

The trendline in Fig. 9 shows a clear linear relationship between the intensity of the reflection and the area of the reflective surface (the facets), as expected. This linear trend in brightness with respect to facet area is impacted by the fact that the illumination of the facets vary, with facets near the top of the prototype (4 mm x 4 mm and 5 mm x 5 mm) angled slightly more towards the sun, thus reflecting slightly more light. All of the data points analyzed to create the

plot were acquired at the same exposure of 1253.25 $\mu$s and were taken from the same camera to prevent discrepancies resulting from different camera/target angles. The subplots show the mean and the $1\sigma$ standard deviation of the reflected spot intensity profiles; the various colors correspond to the different facet sizes and match the color of the data point for that facet. These profiles show that the reflections have a Gaussian profile, although an image of the sun (a uniform disk) would have been expected if the facets were acting as pinhole cameras. The lack of a crisp, circular image with uniform intensity may be caused by two effects: First, the images may not be far enough from the pinhole to be in focus. Second, images acquired are low resolution (just a few pixels across the image of the Sun) and camera focus or lens aberrations may be blurring the image.

Figure 10 showcases cropped images of the reflection produced by each facet size. In the top row, the intensity clearly scales with the facet size whereas the size of the images is mostly unchanged, as detailed below. All cropped regions were taken from the same image at an exposure of 1253.25$\mu$s when the DISCOBaLL was 1.83 m from the flat panel. The top row of images have had a background and dark noise subtraction applied but are otherwise unscaled from the raw data in terms of intensity. At first glance, the reflection size of the images appears to increase with facet size. This perceived trend is due to the dimmer Gaussian shape object having edges that fall below our eye's detection limits; the spots in reality are similar in size despite being much different in intensity. The bottom row of cropped images in Fig. 10 were produced by taking the background and dark noise subtracted images from the top row and normalizing each cropped image by the maximum grey value of the image. After this intensity normalization is performed, it becomes more obvious that all of the reflections produced by the DISCOBaLL are similar in size. This observation again reaffirms the hypothesis that the facets are acting as a pinhole camera producing an image of the Sun because the facet size is only dependent on relative distance from the object and the image to the pinhole. These distances are the same for each of the facet regions on the Version 2.0 prototype. Quantified results supporting this statement are presented later in the current section. Figure 10 also showcases the light bridging effect described earlier in this section. In the background subtracted and normalized images of the 2 mm $\times$ 2 mm and 3 mm $\times$ 3 mm facet reflections the light bridges can clearly be seen as the low grey value lines connecting the reflections in the vertical direction. These vestiges of the manufacturing process become more problematic as the density of the reflections increases. When looking at the 2 mm $\times$ 2 mm normalized image, the light bridging is much more apparent than in the 3 mm $\times$ 3 mm normalized image. As stated earlier, this light bridging effect was exacerbated in the vertical direction due to the curvature of the surface being less severe along that axis than the horizontal axis, possibly resulting in more polishing and rounding of those edges. Consequently, in this analysis horizontal lines of pixels were sampled to create the average intensity profiles instead of vertical lines.

Figure 11 shows the measured reflection diameter versus the area of the reflective surface to provide some quantitative context to the qualitative observations made in Fig. 10. First, the data was sampled from both distance data sets (0.59 m and 1.83 m) using the same methods as the results in Fig. 9 (thresholding, binarization, and taking a horizontal intensity profile). In addition to sampling the reflections from the DISCOBaLL facets, the mirrors of 0.5", 1", and 2" diameter were sampled. A photogrammetry measurement using the stereo camera images was performed to find the distance from the camera to the location of the flat board. Using this distance value, the spatial resolution of the 2048 $\times$ 1536 pixel image plane was estimated in each direction. The spatial resolution in the horizontal direction is denoted by $k_{\mathrm{h}}$ and has a value of 1.51 mm/pixel for the 0.59 m data set and 2.45 mm/pixel for the 1.83 m data set.

For each horizontal line of pixels sampled, a curve representing the reflection intensity profile was generated in the same manner as data processing described for Fig. 9. The full width of the curve at half the maximum (i.e., FWHM) was calculated for each DISCOBaLL reflection intensity profile as well as the mirror reflections, yielding the reflection diameter in pixels. For the DISCOBaLL reflections, all of the FWHMs for each facet size were averaged together and the standard deviation was calculated. All of the FWHMs were then multiplied by the respective horizontal spatial resolution to determine the reflection diameter in mm, which is potted vs. facet area in Fig. 11 using the same color convention as the Fig. 9 data. For each $d_s$ test condition, Eq. 10 was used to estimate the expected reflection diameter; these are plotted as horizontal lines on Fig. 11. The dashed horizontal line represents the predicted reflection diameter at $d_s$ = 0.59 m and the dash-dot horizontal line represents the predicted reflection diameter at $d_s$ = 1.83m. The $1\sigma$ standard deviation is plotted in the error bars on all of the DISCOBaLL data points.

For each $d_s$ the DISCOBaLL points fall close to the predicted reflection size (within 15.1% for the $d_s$ = 0.59 m case and within 21.2% for the $d_s$ = 1.83 m case). The 4 mm and 5 mm facet sizes show slightly larger computed reflection diameters, which is likely due to the fact that the flat panel was slightly tilted when the data was collected and caused the distance from the DISCOBaLL to the flat panel to be slightly shorter for the 2 mm and 3 mm facets than for the 4 mm and 5 mm facets. Additionally, the camera was higher than the center of the flat panel and therefore viewing the facet reflections from an angle and from slightly further away, affecting their perceived size. Deviations from the predicted size may be due to error propagating through the measurement from a few sources, namely: the elliptical appearance of

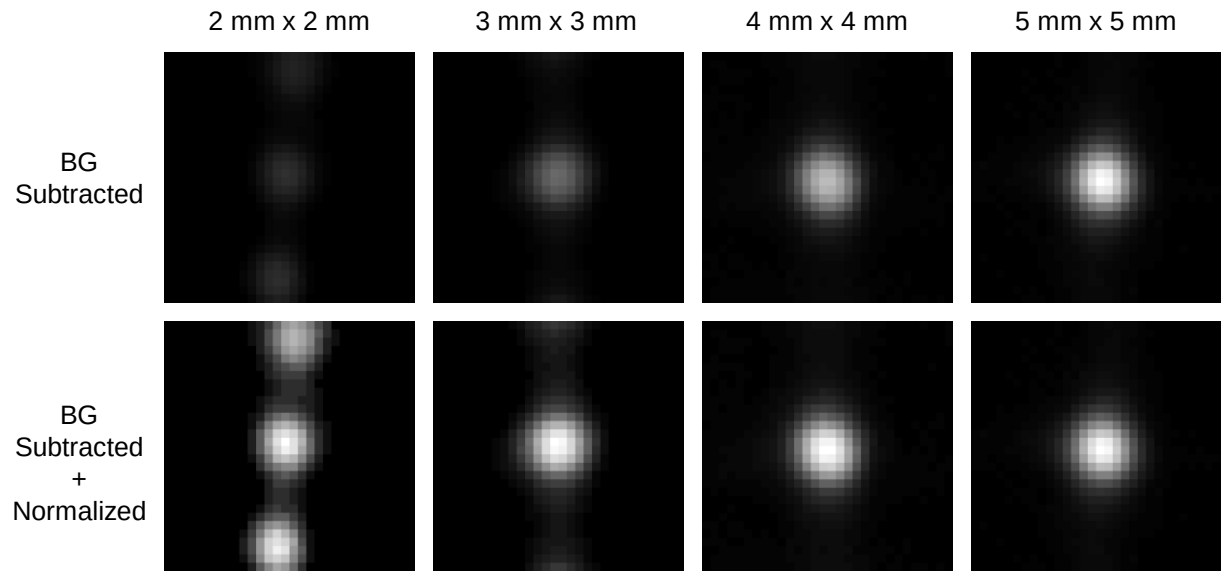


**Fig. 10 Table containing cropped images of the DISCOBaLL prototype Version 2.0 reflections acquired at a distance of 1.83 m from the flat panel. Facet size is increasing from left to right. The top row contains the raw signal which has had the background and dark noise subtracted. The bottom row is the top row of images normalized against the peak intensity of the cropped image. The size of the reflections appear different to the eye in the upper row, but upon normalization the reflections look similar in size.**

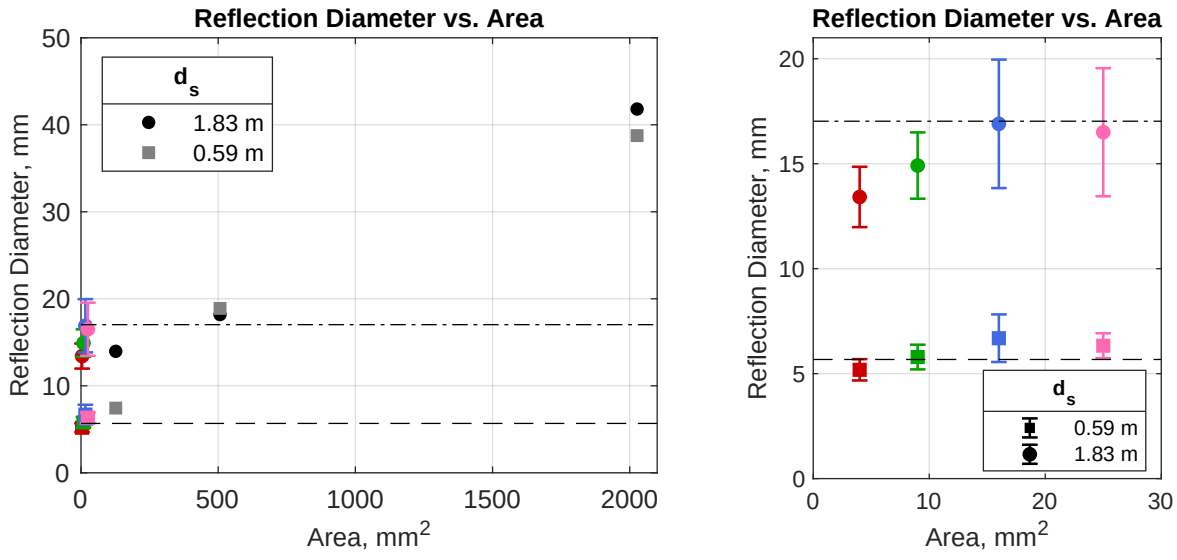


**(a)** **(b)**

**Fig. 11 Plot showing the size of the reflections versus the area of the reflective surface for DISCOBaLL prototype Version 2.0. The dashed and dashed-dotted horizontal lines represent the predicted size of the image of the Sun at 0.59 m and 1.83 m respectively, based on equation 10. (a) Overall plot including DISCOBaLL and mirror reflection sizes. (b) Smaller plot zoomed in on the DISCOBaLL region.**

the reflection to the camera, the fact that the orientation of the flat panel was not straight-on relative to the camera,

and the first-order approximation of the spatial resolution. Another potential source of error could be defects in the manufacturing process, but not enough testing has been done to assess the impact of part precision.

Additional evidence that the DISCOBaLL reflections act as a pinhole aperture producing an image of the Sun lies in the acquired imagery and reflection size measurements. When observing the 0.5" mirror, a large difference can be seen in the measured reflection diameter from $d_s$ = 1.83 m to 0.59 m. When the flat panel is 0.59 m from the testing apparatus, the 0.5" reflection is presenting a reflection diameter more similar to the real reflection size a 0.5" mirror would make if it were forming a true reflection of the mirror surface and not forming an image of the Sun like an aperture. The 0.5" mirror reflection deviates from the actual 12.7 mm diameter reflection size due to the same error sources mentioned above. As $d_s$ is increased, the reflection diameter would be capped at 12.7 mm if the 0.5" mirror were acting as a reflection of the mirror surface. However, the reflection size scales with the same trend as the DISCOBaLL reflections, showing that the 0.5" mirror passes the threshold into the pinhole aperture regime (image distance > 100x pinhole diameter). The other two large mirror spots have some discrepancy between their sizes due to the error effects mentioned before, but the sizes are much more similar than any of the other reflections. This observation provides more evidence that the smaller reflections are acting as an aperture and not forming a true reflection of the reflective surface.

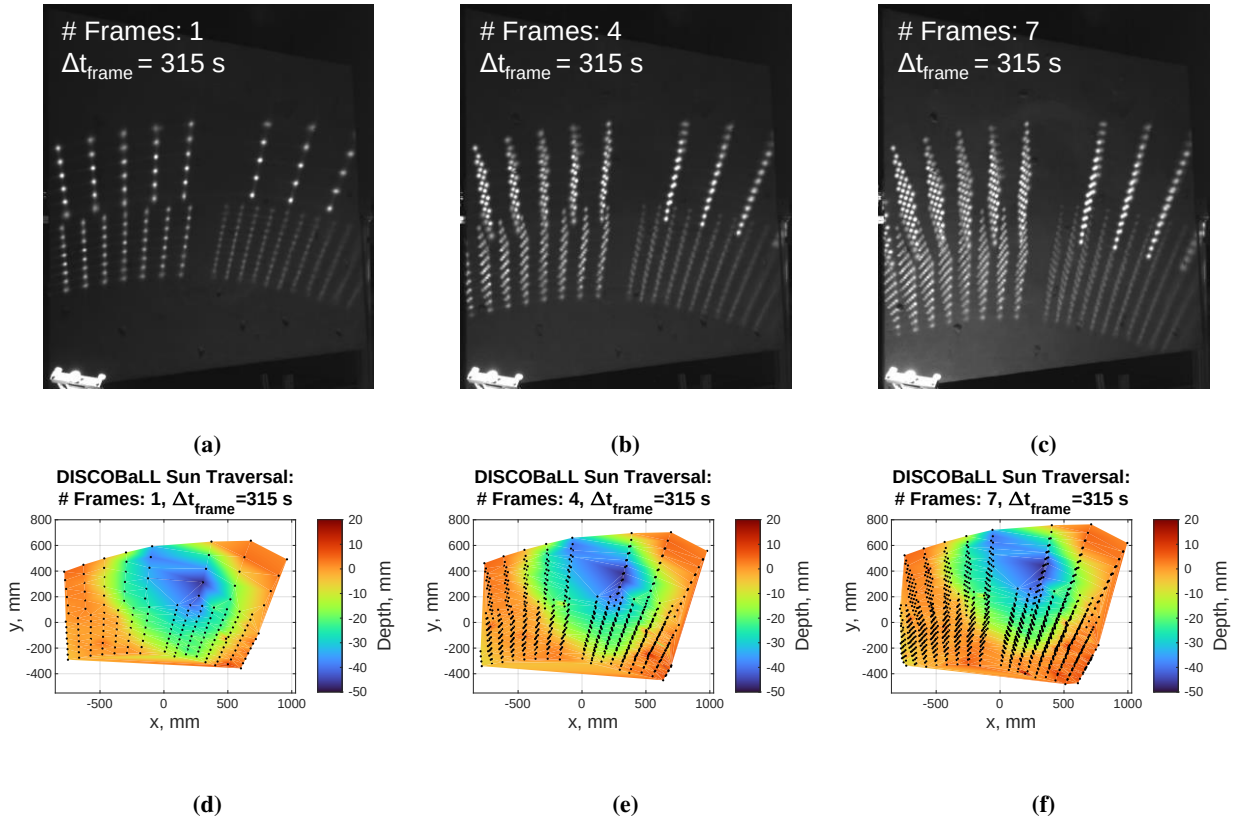


**Fig. 12 DISCOBaLL Sun traversal experiment. Combined single-camera images of DISCOBaLL prototype Version 2.0 spots during sun traversal over (a) 1 frame, (b) 4 frames, (c) 7 frames. Corresponding crater depth maps concatenated over (d) 1 measurement, (e) 4 measurements, (f) 7 measurements.**

The final phase of the DISCOBaLL prototype Version 2.0 testing involved an experiment to test the ability of the SCALPSS system to leverage the Sun traversal over time to improve the measurement, as was demonstrated during the ephemeris simulation described in Section II. As described in Section IV, the DISCOBaLL was set up under the skylight in NASA Langley's MSL to reflect images onto the crater model. The two-camera photogrammetry system was constructed, calibrated and set to acquire images at a frequency of 1 Hz. The setup was then left to acquire data until the sunlight moved completely off of the DISCOBaLL or out of the skylight. In Figs. 12a, 12b, and 12c are images from various points throughout the testing concatenated together. The time between the concatenated images is 315 s. This time interval was chosen such that the DISCOBaLL reflections had enough time to move from their previous location. Note that this DISCOBaLL prototype was not optimized for a Sun traversal experiment, and the range of solar angles

allowed through the laboratory skylight over a relatively short period of time (a few hours) were highly limited. This is why the traversal of the reflections is not as dramatic as the designer GUI prediction for the flight-scale design shown previously in Fig. 4. Figures 12d, 12e, and 12f show the measurements on the lunar crater model created by using the DISCOBaLL reflections in the captured images. As the DISCOBaLL reflections move across the surface of the lunar crater model, new data points are acquired which improve the resolution and fidelity of the measurement. This is evident in Fig. 12f where smaller elevated features (such as rocks) are resolved in the reconstructed depth map and presents a significant improvement over the single-image data shown in Fig. 12d and for the Version 1.0c prototype discussed previously. As the Sun moves across the sky, the DISCOBaLL can capture $N_v \times N_h$ new measurements (minus some of the reflections overlapping with the positions of older measurements) for each successive image sequence collected by the SCALPSS cameras.

## VI. Discussion

Several different illumination options have been identified for future SCALPSS-like instruments to study PSI for missions to the Moon or Mars. These include natural solar illumination [10], DISCOBaLL, laser dots [7, 8], and a laser-sheet illumination method for visualizing the PSI ejecta sheet. Each application is different, and the method(s) selected are mission dependent. Near-equatorial landings may receive appropriate solar illumination to generate high-contrast images over the crater and landing area resulting in high-resolution and accurate pre- and post-landing photogrammetry results. However, landings that occur near dawn or dusk or during the lunar night may not have sufficient illumination even for near-equatorial landings. Worse yet, vehicles that land in a polar region or deep within a large crater may experience darkness beneath the lander, resulting in poor or no photogrammetry measurements without a dedicated illuminator. Such applications would benefit by utilizing the laser-dot illumination or the DISCOBaLL solar illumination. Since the DISCOBaLL requires sunlight, it would not be appropriate for night landings or in deep polar crater missions.

A disadvantage of both the laser-dot illumination and DISCOBaLL schemes is that photogrammetric data is only acquired at the location of the dots. The power of the laser being used (or the physical size of the facets on the DISCOBaLL), combined with the exposure time and gain of the camera, will limit the number of the dots and thus the spatial resolution of the resulting photogrammetry measurements. It is possible that the number of laser dots may be reduced purposely (or the size of the facets increased) so that higher powered light beams may penetrate through the dust cloud, providing measurements during the landing phase which would otherwise be obscured. Such a system would also clearly visualize the location of the top edge of the ejecta sheet as demonstrated in Ref. [8]. To potentially gain back higher spatial resolution, it would be possible to modulate the laser and acquire both solar and laser-illuminated images on alternate frames of the camera by turning off the laser on alternate frames, provided that there is sufficient lighting for non-laser-illuminated images. Note that it would not be possible to modulate the illumination using the DISCOBaLL. However, multiple different DISCOBaLL designs could be flown on a single mission, for example, focused on illuminating the crater from lower and higher altitudes or with different numbers of dots and different intensities.

Another option is for both DISCOBaLL and a laser-based illumination methods (laser dots or laser sheet) to be included on the same mission. For example, the laser-dot illumination method could be used to measure the pre-erosion landing site from high altitude (where the solar images from the DISCOBaLL would be large). Alternately, laser-sheet illumination could provide visualization of the ejecta sheet while the DISCOBaLL illuminates and measures the shape of the crater. The laser could be turned off for some camera acquisitions to allow clear views of the crater with the DISCOBaLL dot illumination.

## VII. Conclusion and Future Work

This paper presents a new passive illumination method that produces multiple images of the sun on the surface of the moon to provide dot-targets for illumination of a lunar crater during and after landing of a lunar spacecraft to study plume-surface interaction. A design tool was developed to predict performance of the reflector. Two prototypes were developed and tested in a laboratory environment, producing encouraging results. Compared to other candidate illumination methods, the main advantage of the DISCOBaLL is in its simplicity, low integration costs, and low risk of failure, though it may be less capable and versatile than laser-dot illumination methods.

To advance the design method to build a full-scale flight prototype, steps will be taken to improve the current design process. These include, but are not limited to, determining the ideal surface milling and finishing technique, enhancing

the fidelity of the advanced features of the modeling GUI, mass reduction, and further testing to characterize the intensity behavior of the reflections. These tools will enable a full-scale flight DISCOBaLL prototype to be designed.

## Acknowledgments

This work was supported by the Stereo Cameras for Lunar Plume-Surface Studies (SCALPSS) Project, which is under the leadership of Robert Maddock as project manager, Chi Nguyen as chief engineer, and Michelle Munk as principal investigator. The SCALPSS project is funded by the NASA Space Technology Mission Directorate (STMD), Game Changing Development (GCD) Program. The authors would like to thank John Angell and the NASA Langley Research Center Metals Application Technology Branch for their support in manufacturing the small-scale DISCOBaLL prototypes. The authors wish to thank the NASA Jet Propulsion Laboratory for the services provided by the Horizons application. The authors wish to thank Dr. Timothy Fahringer for the initial idea of using a disco ball for passive illumination which inspired the present work. The use of trademarks or names of manufacturers in this report is for accurate reporting and does not constitute an official endorsement, either expressed or implied, of such products or manufacturers by the National Aeronautics and Space Administration.

## References

[1] Watkins, R., Metzger, P., Mehta, M., Han, D., Prem, P., Sibille, L., Dove, A., Jolliff, B., Moriarty III, D. P., Barker, D., Patrick, E., Kuhns, M., Laine, M., and Radley, C., "Understanding and Mitigating Plume Effects During Powered Descents on the Moon and Mars," *Bulletin of the AAS*, Vol. 53, 2021. doi:10.3847/25c2cfeb.f9243994.

[2] Mehta, M., Sengupta, A., Renno, N. O., Norman, J. W. V., Huseman, P. G., Gulick, D. S., and Pokora, M., "Thruster Plume Surface Interactions: Applications for Spacecraft Landings on Planetary Bodies," *AIAA Journal*, Vol. 51, No. 12, 2013, pp. 2800–2818. doi:10.2514/1.J052408, URL https://doi.org/10.2514/1.J052408.

[3] West, J., Liever, P., Weaver, A., Shurtz, T. P., Gale, M., Krolick, W. C., and Griffin, L. W., "Overview of the Predictive Simulation Capability Element of the Plume Surface Interaction Project," AIAA SciTech Forum, American Institute of Aeronautics and Astronautics, 2021. doi:10.2514/6.2022-2319, URL https://doi.org/10.2514/6.2022-2319.

[4] Tyrrell, O. K., Thompson, R. J., Danehy, P. M., Dupuis, C. J., Munk, M. M., Nguyen, C. P., Maddock, R. W., Fahringer, T. W., Krolick, W. C., Weaver, A., West, J., Manginelli, M. S., and Witherow, W. K., "Design of a lunar plume-surface interaction measurement system," AIAA SciTech Forum, American Institute of Aeronautics and Astronautics, 2021. doi: 10.2514/6.2022-1693, URL https://doi.org/10.2514/6.2022-1693.

[5] Liu, T., Burner, A. W., Jones, T. W., and Barrows, D. A., "Photogrammetric techniques for aerospace applications," *Progress in Aerospace Sciences*, Vol. 54, 2012, pp. 1–58. doi:10.1016/j.paerosci.2012.03.002, URL https://www.sciencedirect.com/science/article/pii/S0376042112000267.

[6] Jones, T. W., Liddle, D., Banik, J., and Shortis, M., "On-orbit Photogrammetry Analysis of the Roll-Out Solar Array (ROSA)," No. 0 in AIAA SciTech Forum, American Institute of Aeronautics and Astronautics, 2021. doi:10.2514/6.2022-1624, URL https://doi.org/10.2514/6.2022-1624.

[7] Weisberger, J. M., Danehy, P. M., Fahringer, T. W., Bathel, B. F., and Tyrrell, O., "Development of a Terrain Mapping/Crater Evolution Measurement using Diffractive Optical Elements," AIAA AVIATION Forum, American Institute of Aeronautics and Astronautics, 2022. doi:10.2514/6.2022-3562, URL https://doi.org/10.2514/6.2022-3562.

[8] Weisberger, J. M., Danehy, P. M., Fahringer, T., and Tyrrell, O. K., "Evaluation of a Laser-Dot Grid-Projection System for Lunar Lander Crater-Shape and Ejecta-Sheet Measurements," AIAA SciTech Forum, American Institute of Aeronautics and Astronautics, 2024. doi:10.2514/6.2024-1504, URL https://doi.org/10.2514/6.2024-1504.

[9] Contributors, W., "Pinhole Camera — Wikipedia, The Free Encyclopedia," , 2024. URL https://en.wikipedia.org/w/index.php?title=Pinhole_camera&oldid=1258046091.

[10] Tyrrell, O. K., Weisberger, J. M., Fahringer, T. W., Danehy, P. M., and Hutchins, W. D., "Investigating Photogrammetric Accuracy of a Lunar-lander-induced Crater Measurement System," AIAA SciTech Forum, American Institute of Aeronautics and Astronautics, 2023. doi:10.2514/6.2023-2475, URL https://doi.org/10.2514/6.2023-2475.